HHS Public Access

Author manuscript

Opt Lett. Author manuscript; available in PMC 2016 August 25.

Published in final edited form as:

Opt Lett. 2015 November 1; 40(21): 4943–4946.

Volumetric structured illumination microscopy enabled by a tunable-focus lens

Taylor Hinsdale, **Bilal H. Malik***, **Cory Olsovsky**, **Javier A. Jo**, and **Kristen C. Maitland**

Department of Biomedical Engineering, Texas A&M University, 5045 Emerging Technologies Building, 3120 TAMU, College Station, Texas 77843, USA

Abstract

We present a mechanical-scan-free method for volumetric imaging of biological tissue. The optical sectioning is provided by structured illumination, and the depth of the imaging plane is varied using an electrically tunable-focus lens. We characterize and evaluate the ability of this axial-scanning mechanism in structured illumination microscopy and demonstrate its ability to perform subcellular resolution imaging in oral mucosa *ex vivo*. The proposed mechanism can potentially convert any wide-field microscope to a 3D-imaging platform without the need for mechanical scanning of imaging optics and/or sample.

Optical sectioning in high-resolution microscopy is often desirable to improve resolution and contrast. A number of point-scanning optical imaging techniques, such as scanning confocal and multiphoton microscopy, are capable of providing optical sectioning by eliminating out-of-focus light [1,2]. A full 3D volume containing information about a thick sample can be generated by scanning in depth. A wide-field alternative to provide optical sectioning is structured illumination microscopy (SIM), wherein typically three or more images are acquired at preset spatially offset illumination patterns, and out-of-focus light is rejected by mathematical manipulation of the acquired images [3].

The principle of SIM can be represented simply in mathematical terms by describing the intensity of a spatially modulated image as the sum of a uniform intensity image with sinusoidally modulated images. The most basic representation of this is shown in Eq. [1]:

$$I(x,y) = I_c(x,y) + I_s cos(2\pi v_g x + \phi), \quad (1)$$

where $I(x, y)$ is the modulated image as a function of the image plane coordinates x and y, I_c is the intensity image not modulated by the sinusoidal signal, $I_s \cos(2\pi v_g x + \phi)$ is the intensity modulated signal, v_g is the frequency of the modulation pattern in the image plane, and ϕ is the respective phase of the modulation pattern [4]. While I_c is composed of a combination of light before and after the focal plane, the modulated term only strongly exists in the focal plane of the objective. Specifically, higher spatial frequencies are attenuated with defocus. A uniform reconstruction of the light from the focal plane then

*Corresponding author: bilal.malik@qtultrasound.com.

needs to be performed to acquire depth-resolved images. In its most basic form, all that needs to be done to form a sectioned image from images taken of the form in Eq. [1] is to employ a three-phase demodulation technique. This technique can easily be applied by taking three images in which the phase is successively shifted one-third of a period between successive frames [3]. Equation [2],

$$I_p \propto \left[(I_1 - I_2)^2 + (I_1 + I_3)^2 + (I_2 - I_3)^2\right]^{1/2}. \quad (2)$$

can then be employed to reconstruct I_p, or the intensity in the focal plane, where I_1, I_2, and I_3 represent each image in the sequence. Using this method, a faithful reconstruction of the light from the object focal plane can be made while rejecting much of the out of focus light.

In most common embodiments of optical imaging systems, a single in-focus image can be acquired quickly. However, the 3D volumetric acquisition, which requires the process of refocusing to successive image planes, is relatively slower and is one of the limiting factors toward high-speed volumetric image acquisition.

More recently, variable-focal-length lenses have seen considerable utilization towards axial scanning in a multitude of optical-imaging modalities. These include high-resolution imaging techniques, such as multiphoton [5], confocal [6-8], and light-sheet microscopy [9], as well as optical projection tomography [10]. Our group recently reported the use of an electrically tunable lens (ETL) to provide axial scanning in a reflectance confocal microscope [6] and also demonstrated its application and benefits in a clinical device [11].

Here, we present the use of a commercially available ETL wherein the focal length can be varied as a function of the supplied electrical signal to achieve axial scanning in SIM. To the best of our knowledge, this is the first report of the use of a variable-focal-length lens in SIM for imaging biological tissue. We have characterized the optical properties of our SIM, incorporating an ETL and quantified lateral resolution and axial response over the axial scan range of the system. The performance was further demonstrated by imaging of fresh tissue samples from bovine oral mucosa *ex vivo*.

Our SIM system is based on a conventional wide-field geometry utilizing a Ronchi ruling for patterned illumination and an ETL placed just before the objective to enable axial scanning. Figure 1 shows the experimental setup of the system. The system consists of a Kohler illuminated epi-fluorescence microscope. A condenser lens (ACL2520A, Thorlabs, Newton, New Jersey) collects the light from the 455 nm light emitting diode (LED) source (M455L3, Thorlabs) and forms an image on a restricting iris. An image relay (AC254-040-A-ML, AC254-150-ML, Thorlabs) is used to focus the light to the rear focal plane of the objective [40×, numerical aperture NA 0.66, Achromat, Leica]. The fluorescence emitted from the sample is imaged onto a CCD camera (ExiBlue, QImaging, Surrey, BC, Canada) via a 200 mm focal length tube lens (AC254-200-A-ML, Thorlabs). The excitation light is spatially modulated via a 20 line pairs/mm Ronchi ruling (58-777, Edmund Optics, Barrington, New Jersey), which is placed in the middle of the 4f system conjugate, to the focal plane of the objective lens with a magnification between the ruling plane and the object plane of 1/30.

The Ronchi ruling is mounted on a translation stage (T-LSM100A, Zaber, Vancouver, Canada) to enable horizontal movement. To provide axial scanning, the ETL (EL-10-30, Optotune, Switzerland) is placed as close as possible to the rear focal plane of the objective. A 450 ± 20 nm excitation filter (FB450-40, Thorlabs), a 500 nm long pass emission filter (FELH0500, Thorlabs), and a 490 nm cutoff dichroic mirror (DLMP490R, Thorlabs) are used to separate the fluorescence emission from excitation light.

Fresh bovine oral epithelial tissue was acquired from a local butcher shop. Acriflavine hydrochloride (Sigma-Aldrich, St. Louis, MO) was used as a fluorescent contrast agent to stain and visualize the epithelial nuclei. Up to 1 mL of acriflavine solution (0.01% w/v in sterile phosphate buffered saline [PBS]) was applied topically to the tissue with a cotton-tipped applicator for 1 min, rinsed in sterile PBS solution, and imaged immediately. While acriflavine is not yet approved by the US Food and Drug Administration for internal use in the oral cavity, it has a long history of safe clinical use as a topical antiseptic agent and as a fluorescence contrast agent for endomicroscopy [12].

After tissue preparation, the samples were imaged using standard SIM methodology. Three images were taken with the grid pattern shifted one-third of a period relative to the last frame in succession. Combining these images with the SIM phase demodulation technique described in the introduction section removed out-of-focus light and produced optically sectioned images with enhanced signal-to-background ratio.

To test the capabilities of our system, 200 nm subresolution fluorescent microspheres on a thin film were imaged to measure both the lateral resolution and the axial response. Increasing curvature of the ETL is known to increase spherical aberration [6]. To evaluate the effect of the ETL on image quality, measurements of the axial response, the lateral resolution, and the field of view (FOV) were taken over the full range of the axial scan (100 μm), where the ETL scans through a focal length range from 130 mm to 90 mm, corresponding to microscope focal positions defined as 0 μm and 100 μm, respectively. Figure 2 shows the measured axial response (top) and the lateral resolution (bottom) at the distal scan position, where the focal length of the ETL is set to its maximum of 130 mm, and the proximal focal position, where the ETL focal length is 90 mm.

The measurements were made on single spheres near the center of the FOV and normalized by the maximum intensity. For the axial response, the average intensity of a sphere was plotted as it was axially scanned through the focus. For the lateral resolution, the line profile of the sphere at optimum focus was plotted. The FOV and magnification were measured by imaging a Ronchi ruling and then determining the pixels per line pair.

To evaluate these data over the full scan range, the axial response, the lateral resolution, the FOV, and the magnification were measured at three scan positions across the full tunable range, starting with the ETL focal length set at 130 mm, which minimizes the displacement of the focal position from the objectives' nominal working distance. This position is called the 0 μm focal position and is followed by subsequent scanning up to 50 μm and 100 μm in depth. We expected a theoretical axial response of 7.94 μm and a theoretical diffraction limited lateral resolution of 0.46 μm. The expected axial response is calculated using a

spatial frequency response curve that considers the magnification between the grid plane and the sample plane. Using parameters from the physical system, the actual axial response can be numerically calculated [4]. The difference between the expected and measured lateral resolution can likely be attributed to the use of an ETL and, to some degree, the achromatic objective, which introduces additional spherical aberrations. A changing system NA throughout the scan range is another possible cause of the enlarged lateral resolution. Even at the zero scan position, there is still an offset from the nominal working distance, thus an altered NA. The physical size, 200 nm, of the measured microspheres would also affect the lateral resolution, although because they are subresolution, they are not perfect point sources. The measured values are reported in Table 1.

The change in the FOV is caused by the ETL not being placed in the pupil plane of the objective as mentioned earlier. A Zemax model was created to estimate the theoretical shift in focal plane and change in magnification. It consisted of a generic 40× (5 mm focal length) microscope objective model, an official ETL model, and a model of the tube lens used in our system. All these elements were arranged and optimized to be separated from each other with the same distances as in the physical system. Table 1 shows the measured magnification range from 30.5 to 36.2. Using the Zemax model that had the ETL placed 25 mm from the pupil plane of the objective, just as in the physical system, it was shown that over the change in curvature used to scan in our system, the magnification changed from 32.53 to 35.92. Over this full scan range, the focal position exhibited a displacement of 98 μm, which is in relative agreement with the measured 100 μm for the maximum relative displacement. The small differences can likely be attributed to using a generic objective lens model instead of the actual model, which is not provided by the manufacturer. If a lens relay is placed in the Zemax model to image the pupil plane of the objective onto the ETL, the magnification change is greatly reduced. With this simple relay model, it was shown that the magnification changed less than 0.95% over the whole scan range. This can be potentially incorporated in a future system.

To demonstrate the application of our technique in biological tissue, nuclear imaging in bovine epithelial tissue was performed *ex vivo*. The focal plane was axially scanned 100 μm (equivalent to 133 μm when accounting for the refractive index of water in tissue) in depth using the ETL. The scan was performed only in one direction and returned to the starting position at the end of the scan, essentially replicating a sawtooth profile. A maximum intensity projection (MIP) was made over the acquired image stack to show all the in-focus content in the series. Figure 3 shows the MIP images for both the wide-field (top) and the SIM-processed (bottom) data.

Note that when referring to the wide-field images, they are constructed by summing the three structured illumination images, which mathematically represents a wide-field image.

The difference between the SIM-processed images and the wide-field images is apparent in Fig. 3. The details of the stained nuclei and tissue is preserved much better in the SIM MIP when compared with the wide-field MIP; however, this is a qualitative comparison. In the corresponding media file (Visualization 1), the ability of the imaging system to reject out-of-focus light can be clearly observed over multiple planes. Each slice in the 30-image stack

corresponds to a different depth in an equally spaced volumetric scan in which the first image is the plane deepest into the tissue with following slices becoming more superficial.

Multiple cell layers can also be resolved in the image stacks. The depth information is lost in the MIP; however, in the image series (Visualization 1), neighboring nuclei can be seen in and out-of focus at different depths, which is characteristic of optical sectioning techniques. Note that the images in Fig. 3 and corresponding Visualization 1) do not account for change in magnification across the axial scan range. While this did not significantly affect the MIP images for qualitative observation, the varying magnification would need to be taken into consideration for a quantitative feature analysis. The penetration depth was limited in this experiment by the lack of dye penetration deep into the tissue.

Figure 4 shows a close-up view of the effects of SIM processing on in-focus and out-of-focus nuclei from a single image slice. It is clearly seen that out-of-focus nuclei are removed from the image. The SIM images and wide-field images in Fig. 4 were normalized with the same procedure, subtracting the background and scaling the maximum intensity to span the whole dynamic range, to ensure the relative intensities of the in-focus to out-of-focus nuclei could be compared across images. The ratio of the intensity of the in-focus nuclei to the out-of-focus nuclei in Fig. 4(A) improved from 1.62 to 2.35 in Fig. 4(B). This shows an improvement in optical sectioning by rejecting signal from the out-of-focus region.

Topical acriflavine has been shown to have limited penetration and stain only the first couple of superficial epithelial cell layers and have no penetration into deeper layers such as the lamina propria [13,14]. Although the scan range covers a distance 100 μm, features are only resolvable over the first two cell layers, corresponding to an imaging depth between 15 and 20 μm.

The advantage of this SIM system with ETL is that it can create optical sections and scan axially without any mechanical means. This provides the microscope with greater flexibility for *in vivo* use and the potential to be incorporated into an endoscopic system, especially with the advent of smaller tunable lenses [15]. Note that SIM has also been used for resolution enhancement. This can be achieved by increasing the number of structured illumination patterns at different orientations and phases. While the current optical resolution of our presented imaging system is adequate for tissue-level imaging, it can be potentially further increased for subcellular imaging [16].

One drawback of using ETLs is that typically they are not well corrected for aberrations at all focal lengths across the scanning range, which can lead to reduced and varying image quality with greater curvature, as seen in the results above, resulting in discrepancies in theoretical and measured parameters. The ETL also introduced slight magnification errors, which can be seen as a change in the FOV in Table 1. As mentioned earlier, this is due to the ETL not being in the rear focal plane of the objective. In addition, any change in divergence or convergence of the beam (by tunable lens) changes the effective NA of the system, potentially contributing to the dis-agreement in modeled and measured values of optical resolution. This can potentially be solved by using an image relay to image the rear focal plane of the objective onto the ETL [10].

The acquisition of phase-shifted images in our system requires movement of the Ronchi ruling, which is the limiting factor in our image grid translation accuracy. The imperfect translations of the Ronchi ruling can result in images not shifted by exactly one-third of a period, resulting in image artifacts after SIM processing. To address this problem, the translating grid pattern can be replaced with a digital micromirror device (DMD) that utilizes a digitized placement rather than analog [17]. The grid translation rate at ~40 Hz was not a limiting factor for our imaging rate of 0.5 Hz; rather, the exposure time was. The optical layout used in this Letter is specific to this system but the principle of the ETL scanning is easily generalizable to fit most wide-field optical imaging systems.

In summary, we have presented an all optical axial scan method to provide volumetric imaging using SIM within biological tissue. Employing a tunable-focal-length lens can offer a more versatile mechanism for axial scanning within the sample with no relative motion of the microscope objective. In addition, the commercially available tunable lens can be easily retrofitted on most custom-built wide-field microscopes with minimal system changes, or it can be added in a conjugate image plane in more restrictive commercial microscopes.

Acknowledgment

The authors would like to thank Dr. Clay Ashley and his staff at Veterinary Medical Park of Texas A&M with their help in tissue acquisition.

Funding. National Institutes of Health (NIH) (R01 CA138653, R03 CA191860).

REFERENCES

1. Wilson, T., editor. Confocal Microscopy. Academic; 1990. p. 1-64.
2. Jabbour JM, Saldua MA, Bixler JN, Maitland KC. Ann. Biomed. Eng. 2012; 40:378. [PubMed: 21994069]
3. Neil MAA, Juskaitis R, Wilson T. Opt. Lett. 1997; 22:1905. [PubMed: 18188403]
4. Chasles F, Dubertret B, Boccara AC. Opt. Express. 2007; 15:16130. [PubMed: 19550902]
5. Grewe BF, Voigt FF, van't Hoff M, Helmchen F. Biomed. Opt. Express. 2011; 2:2035. [PubMed: 21750778]
6. Jabbour JM, Malik BH, Olsovsky C, Cuenca R, Cheng S, Jo JA, Cheng Y-SL, Wright JM, Maitland KC. Biomed. Opt. Express. 2014; 5:645. [PubMed: 24575357]
7. Koukourakis N, Finkeldey M, Stürmer M, Leithold C, Gerhardt NC, Hofmann MR, Wallrabe U, Czarske JW, Fischer A. Opt. Express. 2014; 22:6025. [PubMed: 24663938]
8. Riza NA. Opt. Eng. 2008; 47:063201.
9. Fahrbach FO, Voigt FF, Schmid B, Helmchen F, Huisken J. Opt. Express. 2013; 21:21010. [PubMed: 24103973]
10. Chen L, Kumar S, Kelly D, Andrews N, Dallman MJ, French PM, McGinty J. Biomed. Opt. Express. 2014; 5:3367. [PubMed: 25360356]
11. Jabbour JM, Bentley JL, Malik BH, Nemechek J, Warda J, Cuenca R, Cheng S, Jo JA, Maitland KC. Biomed. Opt. Express. 2014; 5:3781. [PubMed: 25426310]
12. Fuchs FS, Zirlik S, Hildner K, Schubert J, Vieth M, Neurath MF. Eur. Respir. J. 2013; 41:1401. [PubMed: 22997220]
13. Neumann H, Kiesslich R, Wallace MB, Neurath MF. Gastroenterology. 2010; 139:388. [PubMed: 20561523]
14. Polglase AL, McLaren WJ, Skinner SA, Kiesslich R, Neurath MF, Delaney PM. Gastrointest. Endosc. 2005; 62:686. [PubMed: 16246680]

15. Ozbay BN, Losacco JT, Cormack R, Weir R, Bright VM, Gopinath JT, Restrepo D, Gibson EA. Opt. Lett. 2015; 40:2553. [PubMed: 26030555]
16. York AG, Parekh SH, Dalle Nogare D, Fischer RS, Temprine K, Mione M, Chitnis AB, Combs CA, Shroff H. Nat. Methods. 2012; 9:749. [PubMed: 22581372]
17. DMD 101: introduction to digital micromirror device (DMD) techology. Texas Instruments Inc.; 2013. Application Report DLPA008A

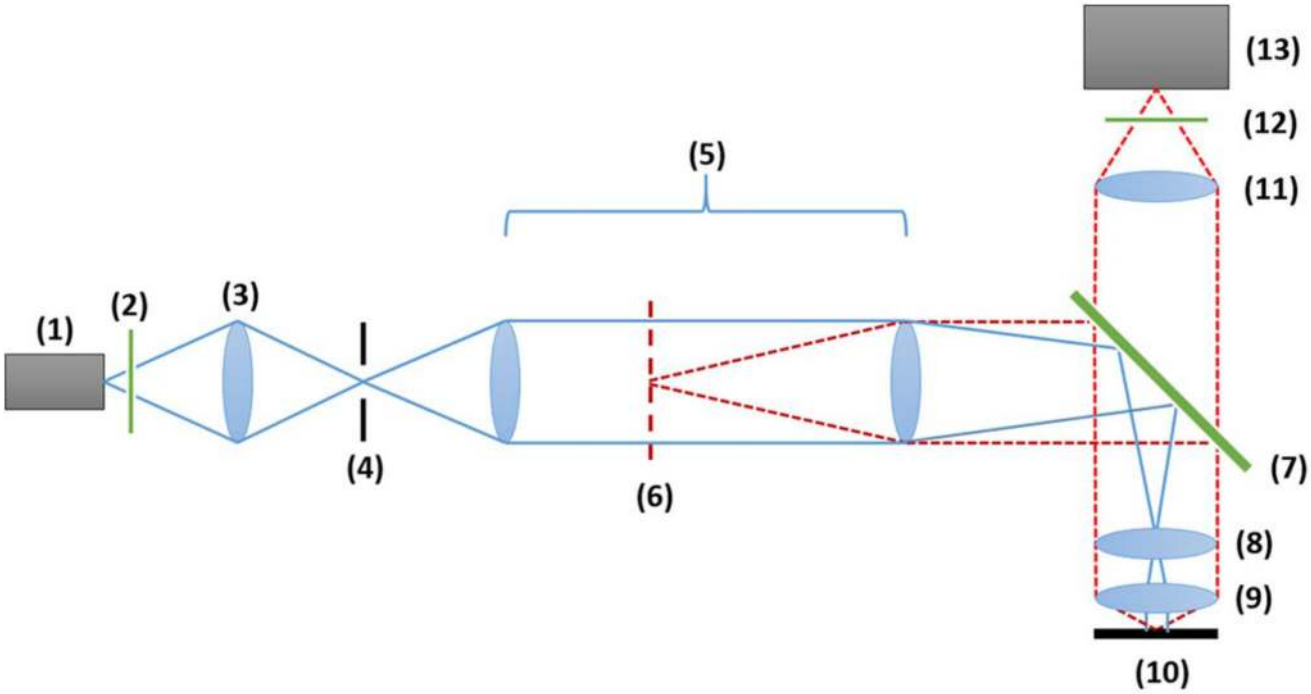

Fig. 1.

SIM system schematic. (1) LED, (2) excitation filter, (3) condenser lens, (4) condenser aperture, (5) image relay, (6) Ronchi ruling, (7) dichroic mirror, (8) tunable lens, (9) objective lens, (10) sample plane, (11) tube lens, (12) emission filter, (13) CCD camera.

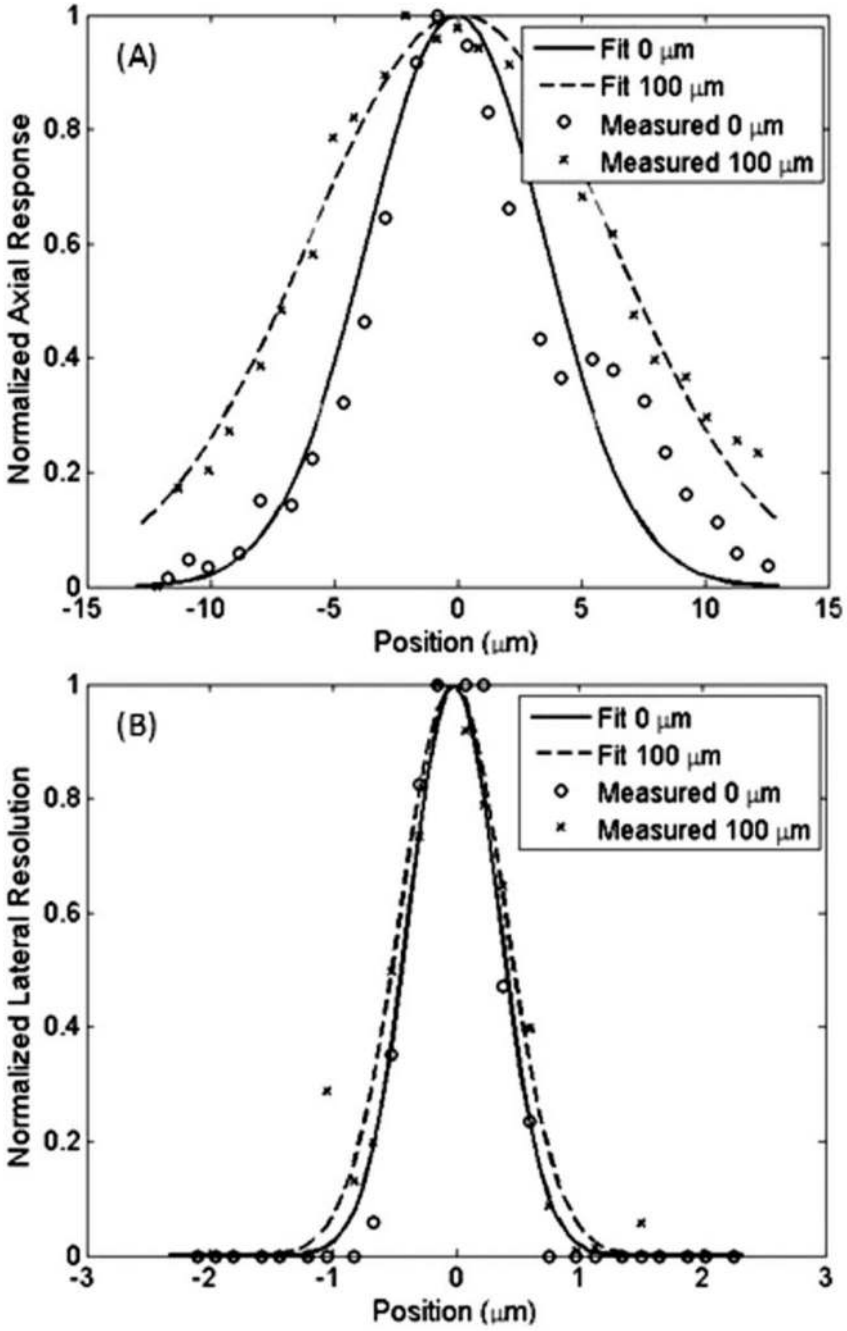

Fig. 2.

(A) Axial response of SIM at 0 and 100 μm scan distance. Using a Gaussian fit, the full-width-half-maximum (FWHM) of the axial response is 7.95 and 14.13 μm, respectively. (B) Lateral resolution of the optical system at 0 and 100 μm scan distance. Using a Gaussian fit, the FWHM of the lateral response is 0.78 and 1.14 μm, respectively.

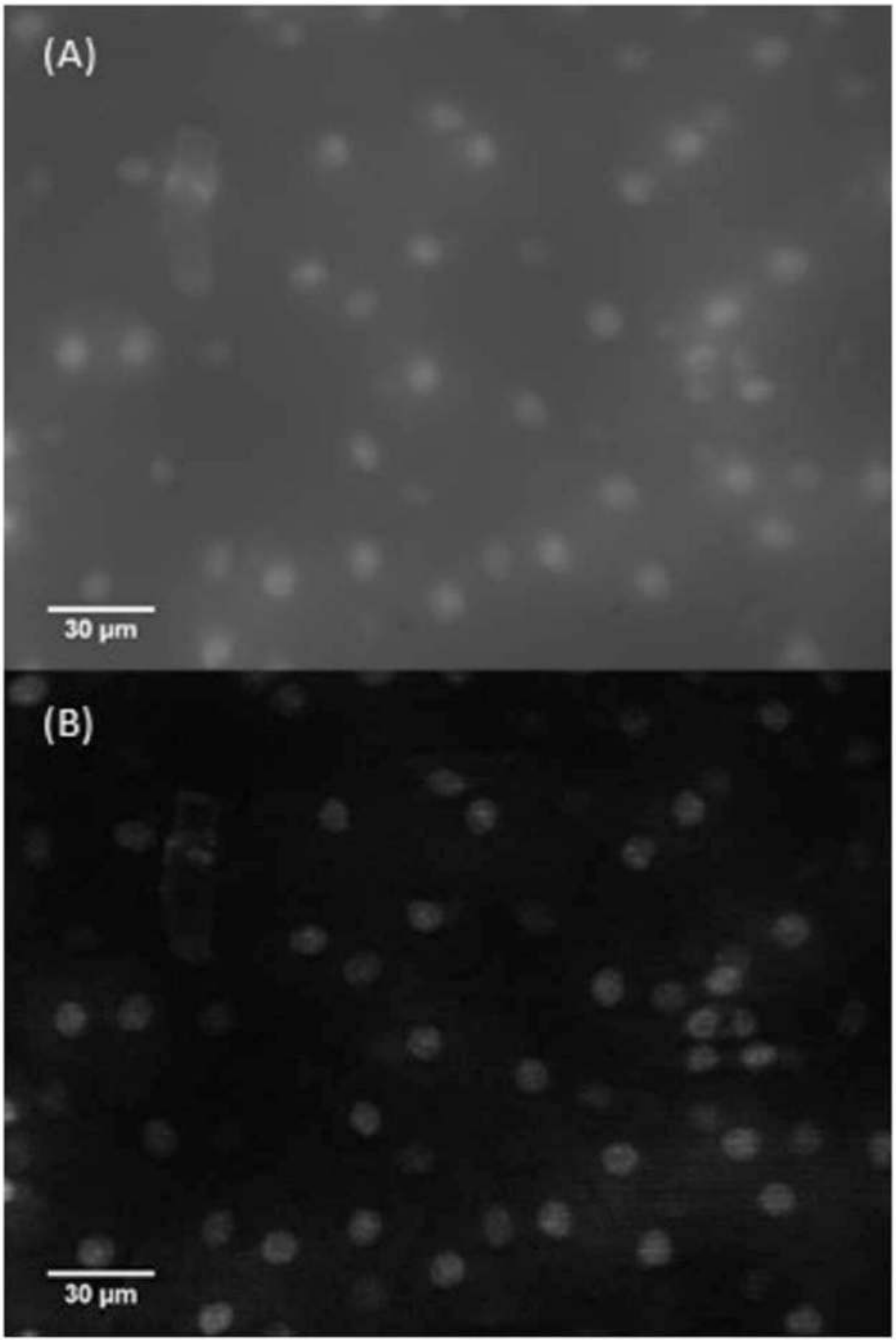

Fig. 3.

Comparison of (A) wide-field microscopy and (B) SIM image of oral mucosa stained with acriflavine; Both A and B are MIP images created from 133 μm axial scan using an ETL and (Visualization 1) raw image stacks.

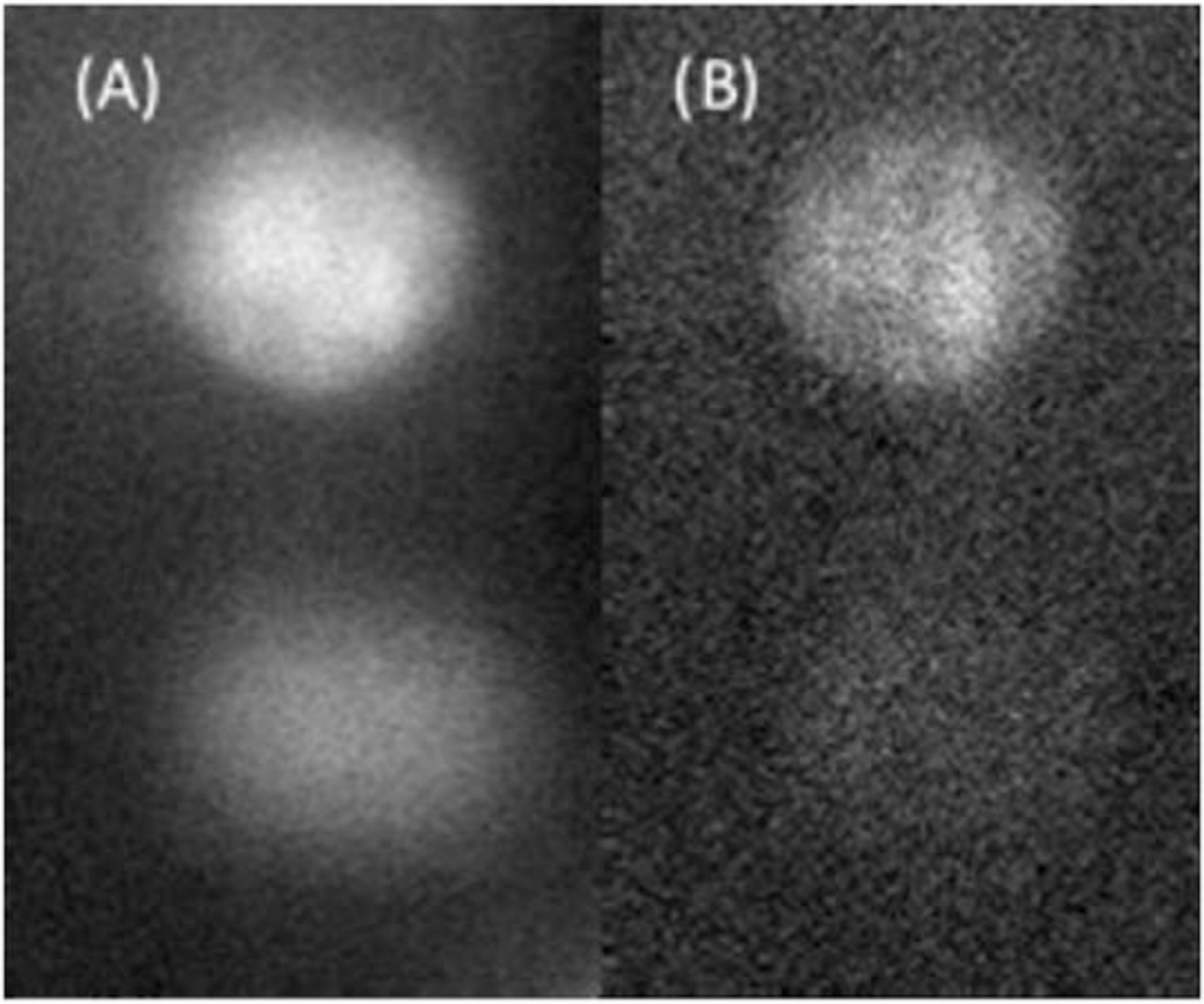

Fig. 4.

(A) Single pre-SIM processing image slice and in-focus nuclei, top, and out of focus nuclei, bottom; (B) SIM of oral mucosa stained with acriflavine showing the removal of the out of focus nuclei.

Table 1

Imaging parameters[a]

FPa (μm)	0	−50	−100
AR (μm)	7.95 (0.84)	10.55 (1.56)	14.13 (0.22)
LR (μm)	0.78 (0.1)	0.93 (0.08)	1.14 (0.19)
FOV (μm^2)	248 × 185	268 × 200	293 × 219
M	30.5	33.4	36.2

[a]FP, focal position; AR, axial response mean (standard deviation); LR, lateral resolution mean (standard deviation); FOV, field of view (FOV); and M, magnification.